GEOPHYSICS, VOL. 90, NO. 1 (JANUARY-FEBRUARY 2025); P. 1–14, 14 FIGS., 2 TABLES.
10.1190/GEO2023-0767.1

NeRSI: Neural implicit representations for 5D seismic data interpolation

Wenbin Gao[1], Dawei Liu[2], Wenchao Chen[1], Mauricio D. Sacchi[3], and Xiaokai Wang[1]

ABSTRACT

Due to challenging field operations and resource constraints, seismic data acquisition often requires coping with missing traces. Interpolation algorithms are crucial for reconstructing these missing traces to enable improved subsurface analysis and interpretation. Although deep learning has made exciting advances in seismic reconstruction, its focus has predominantly been on 2D and 3D data sets with relatively low rates of missing data. Reconstruction of 5D seismic data entails considering simultaneous sources and receivers deployed in areal arrays to solve the reconstruction problem. The latter offers greater data redundancy, which can be leveraged to enhance interpolation quality. Traditional 5D deep-learning interpolation methods rely heavily on synthetic training pairs, posing challenges when applied to real-world data. This necessitates transfer learning techniques, which can be cumbersome. To address this, we introduce a self-supervised, coordinate-based deep interpolation algorithm that mitigates the need for labeled data. Using a multilayer perceptron (MLP) network can effectively encode the continuous seismic 5D wavefield. Once trained, the MLP can infer missing trace amplitudes from their coordinates. We contribute to boosting the MLP, enabling it to generate seismic profiles rather than single-point predictions. This enhancement significantly strengthens the model's performance and efficiency. Moreover, we apply nuclear norm regularization to the output profiles, improving the reconstruction quality. The effectiveness of our algorithm is illustrated with synthetic and field data experiments.

INTRODUCTION

In exploration seismology, seismic data with complete sampling are essential for subsequent tasks, such as amplitude-variation-with-offset analysis (Downton et al., 2010), simultaneous source separation (Zhou et al., 2016), and fault detection (Wu et al., 2019a, 2019b). However, limitations imposed by physical or economic factors often result in missing traces in the observed data. Therefore, it is imperative to appropriately restore data and reconstruct a complete and continuous wavefield (Chen et al., 2016). Otherwise, these missing traces, carrying valuable geologic information, will adversely affect subsequent data processing and interpretation. Therefore, seismic data reconstruction has attracted considerable attention from academia and industry in the past several decades.

Traditional methods consider seismic interpolation problems to be typical underdetermined inverse problems that do not have a unique solution. It is necessary to impose constraints in the interpolation process to obtain the most realistic reconstruction result.

The first category is methods based on predictive filters. Considering the predictability of linear events in seismic data, the *f-x* domain prediction error filter method (Spitz, 1991; Porsani, 1999; Naghizadeh and Sacchi, 2009) is proposed, and this method is subsequently extended to the *t-x* (Crawley et al., 1999) and *f-k* domains (Gulunay and Chambers, 1996). With the prediction error filter-based approach, the missing traces can be interpolated by filters derived from nonaliased low-frequency data (Liu et al., 2022). Although quite effective, these methods require the manual adjustment of parameters such as the length of the filter and window size to meet the linear-events assumption.

The second category comprises rank-reduction-based approaches, which assume that the complete data are inherently low rank. Meanwhile, the presence of missing traces increases the rank of the required matrix or tensor. In this regard, seismic data interpolation can be viewed as a low-rank matrix or tensor completion problem. Matrix-based approaches entail organizing spatial data at a given temporal

Manuscript received by the Editor 20 December 2023; revised manuscript received 16 September 2024; published ahead of production 7 October 2024.
[1]Xi'an Jiaotong University, School of Information and Communications Engineering, Xi'an, China. E-mail: 1816364944@qq.com; wencchen@xjtu.edu.cn; xkwang@xjtu.edu.cn.
[2]Xi'an Jiaotong University, School of Information and Communications Engineering, Xi'an, China and University of Alberta, Department of Physics, Edmonton, Alberta, Canada. E-mail: 409791715@qq.com (corresponding author).
[3]University of Alberta, Department of Physics, Edmonton, Alberta, Canada. E-mail: msacchi@ualberta.ca.

frequency into block Hankel/Toeplitz matrices or texture matrices and then applying a rank reduction algorithm such as truncated singular value decomposition (SVD) to fill empty traces (Trickett et al., 2010; Oropeza and Sacchi, 2011; Gao et al., 2013; Chen et al., 2016). In parallel, numerous studies have already leveraged the low-rank properties of tensors for seismic data recovery, such as the high-order SVD (Kreimer and Sacchi, 2012), Tucker decomposition (Da Silva and Herrmann, 2015), and tensor SVD (Ely et al., 2015). By leveraging tensor unfoldings and matrix factorization technologies, Gao et al. (2015) adopt the parallel matrix factorization (PMF) algorithm (Xu et al., 2015) to reconstruct a low-rank tensor structure from undersampled seismic data. This technique performs matrix factorizations to the different tensor unfoldings, thus dramatically decreasing the computational complexity by avoiding the use of SVD. Following this, Liu et al. (2022) incorporate tensor ring (TR) rank unfolding and further develop PMF-TR. Tensor-based approaches preserve the seismic waveforms better because all physical dimensions of the seismic data are considered, demonstrating the inherent potential of tensor algebra for developing new reconstruction techniques.

As a third category, transform-based methods play a pivotal role in addressing the issue of recovering missing traces. The Fourier transform with simple constraints, such as band-limited wavenumber-domain regularization and the sparsity-promoting regularization of spectral amplitudes, is widely used by the industry (Liu et al., 2022). The sparsity-promoting methods assume that complete seismic data exhibit sparsity in a specific transformation domain, such as the Radon (Bardan, 1987; Kabir and Verschuur, 1995; Chen et al., 2021b), shearlet (Liu et al., 2019b), seislet (Fomel and Liu, 2010; Gan et al., 2015), or curvelet (Hennenfent et al., 2010; Shahidi et al., 2013; Wang et al., 2015) domains. Then, the presence of missing traces disrupts this sparsity. Therefore, it becomes possible to recover missing traces by enhancing the sparsity of the data in the transform domain. However, these methods require predetermined transforms and the fixed transforms may not adapt well to complex data. To refine it, researchers introduce dictionary learning methods that adaptively derive a group of atoms to better fit the data and preserve their subtle features, involving K-SVD (Zhu et al., 2015; Wang et al., 2021) and data-driven tight frame methods (Yu et al., 2015). Nevertheless, these methods tend to be computationally intensive and sensitive to parameter selection, rendering them unaffordable when dealing with high-dimensional problems.

Nowadays, deep-learning techniques demonstrate their remarkable potential across various domains, and seismic data interpolation is no exception. Unlike traditional methods, supervised deep-learning algorithms can acquire prior knowledge by learning from a training data set (Liu et al., 2019a; Yu et al., 2019). In addition, owing to the utilization of nonlinear activation functions, neural networks can effectively capture nonlinear features within the data, yielding enhanced information extraction and representation capabilities. Currently, various types of neural networks have been used in seismic data interpolation, including autoencoders (Mandelli et al., 2018; Wang et al., 2020), generative adversarial networks (GAN) (Oliveira et al., 2018; Siahkoohi et al., 2018), and model-driven networks (Zhang et al., 2020a; Xu et al., 2022). Although neural networks demonstrate promising results in seismic data interpolation, they mainly concentrate on low-dimensional data, such as 2D or 3D seismic data. Moreover, many of these methods rely on synthetic data for supervised training, thereby constraining the model's performance to the quality of the training data.

Various unsupervised seismic interpolation methods have emerged to address the challenges of insufficient training labels in recent years. Fang et al. (2023a) introduce a novel self-supervised learning interpolation network (SSLI) inspired by Noise2Void (Krull et al., 2019). SSLI samples a small portion of the trace from the missing data as a label and uses the remaining part of the missing data to predict the sampled segment. Subsequently, a vast number of samples from the missing data are randomly selected to train the Unet-like network. Upon completion of the training process, the original missing data are used to predict the corresponding complete data, yielding promising results in 2D and 3D data. Kong et al. (2020) propose an unsupervised 3D seismic data interpolation network called deep-prior-based seismic data interpolation (DPSI). This approach involves feeding random noise into a multiscale Unet network to fit the observation data at the observed locations. In addition, the authors introduce an adaptive weighted Laplacian regularization term to constrain the network's output, thereby achieving unsupervised 3D seismic data interpolation.

In contrast to 2D/3D data, 5D seismic data can represent the directionality of geologic features and the changes in seismic responses with different offsets and azimuths, leading to a better understanding of the subsurface properties. However, characterizing complex geologic settings in 5D data with deep learning faces unique challenges. First, the computational resources required for 5D convolution are more significant than for three dimensions. Then, common deep-learning frameworks such as TensorFlow and PyTorch do not have 5D convolution operators, preventing their use for 5D data processing. To mitigate this, Fang et al. (2023b) use the characteristics of 3D convolution operations to construct a 5D convolutional neural network. Subsequently, synthetic 5D seismic data are used as labels to train this network, enabling it to perform data interpolation. However, further enhancements to computational efficiency are necessary for this method to gain widespread usage. In summary, developing an efficient, label-free, and robust 5D reconstruction method is essential for real-world scenarios and remains an area of ongoing exploration.

Computer vision has witnessed significant advancements with the introduction of neural implicit representations, which use neural networks to learn continuous functions mapping spatial coordinates to physical attributes. Originally applied to computer vision tasks such as scene representation (Martin-Brualla et al., 2021; Mildenhall et al., 2021), image processing (Xu, 2020; Chen et al., 2021d), and 3D object representation (Mohamed and Lakshminarayanan, 2016; Park et al., 2019), neural radiance fields (NeRF) are particularly influential. These models comprise a Fourier feature mapping (FFM) module and a multilayer perceptron (MLP) network, enabling us to encode the wavefield point-wise. Specifically, the FFM module proficiently converts spatial coordinates into Fourier domain encodings, and the MLP correspondingly maps these Fourier encodings to their respective values. This way, the complete and continuous wavefield information becomes encoded within the MLP's weight parameters by training the model using observed data points. Consequently, the missing data can be reconstructed by querying the values corresponding to the respective coordinates. The neural representations for videos (NeRV) framework (Chen et al., 2021a) further enhances the efficiency of NeRF-based methods by transitioning from point-wise to image-wise processing, significantly accelerating encoding and decoding speeds while maintaining high-quality outputs.

Although these neural implicit representations have demonstrated effectiveness in computed tomography (CT) reconstruction (Sun et al., 2021) and seismic interpolation (Goyes-Peñafiel et al., 2023; Li et al., 2024; Liu et al., 2024), their accelerated adaptation to 5D seismic data remains underexplored. This paper extends NeRV (Chen et al., 2021a) to achieve an efficient reconstruction of the missing traces within 5D seismic data. Specifically, we propose neural implicit representations for seismic interpolation (NeRSI) — specially engineered for reconstructing 5D seismic data. Our approach is characterized by a novel, coordinate-based, profile-wise framework that captures the complex structural characteristics of 5D seismic signals. A convolutional neural network component is at the heart of this framework, functioning as a decoder to reconstruct complete seismic profiles. This method departs from traditional point-based techniques (Li et al., 2024; Liu et al., 2024), significantly enhancing training and testing efficiency. In addition, we add a nuclear norm regularization item to improve the model's resistance to noise, thus effectively exploiting the intrinsic properties of 5D seismic signals. Synthetic and field data examples illustrate the efficacy of NeRSI. The core contributions of this research are as follows.

1) An efficient 5D seismic data reconstruction approach with a self-supervised coordinate-based internal learning method is developed, eliminating the need for additional labeled data. To our knowledge, this is the first attempt accelerating an approach in 5D seismic data processing.
2) Building upon the original point-wise approach in NeRF, we propose an advanced profile-wise technique that fully exploits the unique properties of seismic data. This enhancement results in a substantial 40-fold increase in data processing efficiency, enabling a faster and more accurate reconstruction of 5D seismic data.
3) To further improve the robustness of our model, a nuclear norm regularization is added to our objective function, significantly enhancing its robustness to noise.

METHOD

Neural network implicit representation for 5D interpolation

In seismic data interpolation algorithms, the predominant emphasis has historically been placed on manipulating 2D and 3D data sets. However, the intricate nature of 5D seismic data, which incorporate offset and azimuths, provides a more complete representation of seismic data. This enrichment of the data structure enhances the fidelity of seismic interpretation and introduces a beneficial level of redundancy conducive to more sophisticated interpolation techniques. Despite these advantages, interpolating 5D data remains a formidable challenge due to the prestack nature of these datasets and the substantial computational costs from their large volume. This study aims to directly address these obstacles to fully harness the rich information embedded within 5D seismic data.

This paper emphasizes the essential process of regular 5D data interpolation. The binned seismic data are structured into a 5D tensor for enhanced analysis and clarity, as shown in Figure 1. For source-receiver coordinates, entries in the observed tensor can be expressed as $\mathcal{D}^{\text{obs}}(t, s_x, s_y, r_x, r_y)$, where (s_x, s_y, r_x, r_y) are the source and receiver locations. With a different data sorting, in midpoint-offset, the entries can also be denoted as $\mathcal{D}^{\text{obs}}(t, m_x, m_y, h_x, h_y)$. Here, t represents time, m_x and m_y represent the inline and crossline midpoint coordinates, and h_x and h_y indicate the inline and crossline offsets, respectively. Alternatively, the data can be arranged as $\mathcal{D}^{\text{obs}}(t, m_x, m_y, |\mathbf{h}|, \alpha)$, where $|\mathbf{h}|$ represents the absolute offset, and α signifies the azimuth. For a general representation, the preceding coordinate positions are denoted by a vector $\mathbf{v}$, where a 5D coordinate is expressed as $\mathbf{v} = [v_1, v_2, v_3, v_4, v_5]^{\mathrm{T}}$.

Assuming the observed decimated data $\mathcal{D}^{\text{obs}}$ correspond to the complete data $\mathcal{Z}$, the mathematical relation between $\mathcal{D}^{\text{obs}}$ and $\mathcal{Z}$ can be formulated as follows:

$$\mathcal{D}^{\text{obs}} = \mathcal{P} \circ \mathcal{Z}, \tag{1}$$

where $\circ$ represents the Hadamard (element-wise) product and $\mathcal{P}$ indicates a sampling operator:

$$p_{v_1 v_2 v_3 v_4 v_5} = \begin{cases} 0 & \text{if } d_{v_1 v_2 v_3 v_4 v_5} \text{ is a missing entry} \\ 1 & \text{if } d_{v_1 v_2 v_3 v_4 v_5} \text{ is a nonobserved entry} \end{cases}. \tag{2}$$

Seismic data can be conceptualized as a wavefield, which is essentially a function F mapping coordinates to their respective values in $\mathcal{Z}$:

$$z_{v_1 v_2 v_3 v_4 v_5} = F(\mathbf{v}). \tag{3}$$

As mentioned previously, NeRF is highly effective for representing continuous wavefields. Consequently, we choose to depict the function F using an MLP, denoted as M. By fine-tuning the MLP parameter weights, denoted as θ, we can refine the original equation 3 to

$$z_{v_1 v_2 v_3 v_4 v_5} = M_\theta(\mathbf{v}). \tag{4}$$

Given that the complete data $\mathcal{Z}$ are not directly accessible, our approach involves inferring M_θ using only the observed data $\mathcal{D}^{\text{obs}}$. Hence, our objective function is defined as

$$J_1(\theta) = \sum_{v_1, v_2, v_3, v_4, v_5} E(\mathcal{D}^{\text{obs}}(\mathbf{v}), M_\theta(\mathbf{v})), \tag{5}$$

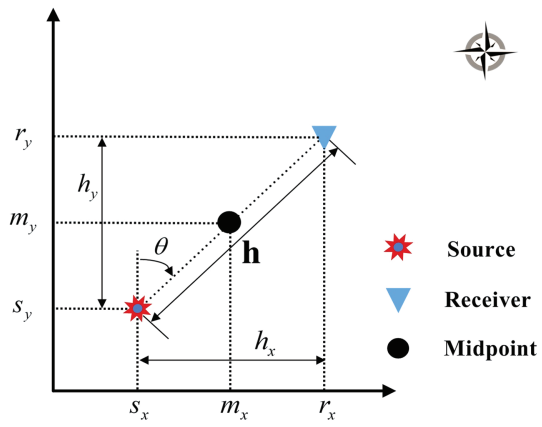

Figure 1. Coordinate system used for describing the 5D seismic data in 3D seismic exploration.

where E represents a distance metric. We adopt the mean-squared error for its simplicity and stability, resulting in the following derived formulation:

$$J_1(\theta) = \sum_{v_1,v_2,v_3,v_4,v_5} \|\mathcal{D}^{\text{obs}}(\mathbf{v}) - M_\theta(\mathbf{v})\|_2^2. \tag{6}$$

Our strategy leverages the inherent continuity of the 5D seismic wavefield as a constraining factor. Fortunately, MLPs exhibit a natural resistance to high-frequency variations. Moreover, this frequency resistance characteristics can be modified by changing the encoding length of input coordinates (Zhang et al., 2020b). Therefore, the inherent prior of MLP guarantees that the learned seismic wavefield encounters the continuity requirements even only training on sparsely sampled $\mathcal{D}^{\text{obs}}$. Subsequently, the complete wavefield $\mathcal{Z}$ can be successfully recovered by querying MLP at each vacant coordinate.

Profile-wise interpolation approach

The technique outlined in equation 6 is referred to as the point-wise method (Liu et al., 2024), with its network architecture shown in Figure 2. This architecture can be characterized as a composition of an encoder, consisting of 16 fully connected layers, and a decoder, comprising two fully connected layers. Although the point-wise method is effective for seismic data interpolation, its single-point output strategy has a notable limitation. This approach treats each point in the wavefield separately, leading to the substantial computational resources required for model training, especially for large data volumes. Moreover, the model tends to inadvertently learn and replicate the noise in scenarios with low signal-to-noise ratio (S/N) field data.

This paper proposes a novel approach, termed the "profile-wise interpolation method," designed to output complete seismic profiles instead of individual pixels. To differentiate it from the point-wise process, we name this technique NeRSI. This method dramatically enhances output efficiency compared with the conventional point-wise approach. In addition, focusing on profile outputs allows us to implement regularization strategies more effectively. Accordingly, the profile-wise interpolation method surpasses the point-wise approach by effectively leveraging the intrinsic correlations within the profiles. This advantage not only amplifies the relevant signals but also significantly boosts the overall performance of the network model. Specifically, to reduce noise in the output data, we integrate nuclear norm loss into the model's loss function. This commonly used loss reduces dependence on self-supervised training data and makes use of prior knowledge to place constraints on the output profiles, markedly improving the accuracy of the interpolation process.

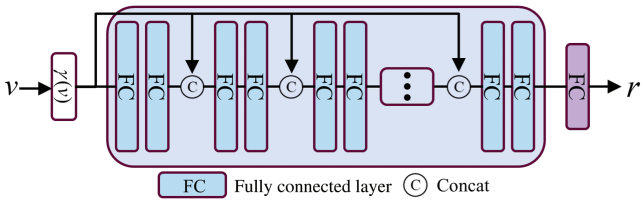

Figure 2. MLP network structure for the point-wise interpolation method.

Profiles characterized by well-defined structural information and stable event continuity are particularly suitable for convolutional network learning. This stems from the inherent nature of convolutional operations, which extract features with more predictability and regularity. Therefore, selecting an appropriate output profile dimension is crucial in the proposed profile-wise approach because our seismic data have five dimensions. To achieve this, we explore two different scenarios. For seismic data without normal moveout (NMO) correction, we specifically select one data gather that displays continuous events and clear structures. As an illustrative example, we refer to the SEG C3_NA open data set (Society of Exploration Geophysicists, 2024), which is organized in source-receiver positions. Through careful examination, we fix s_x, s_y, and r_x, resulting in the output gather, denoted as $\mathcal{D}^{\text{obs}}(:, s_x, s_y, r_x, :)$. The colon notation $(:)$ indicates that the tensor is being sliced along the first and last dimensions, meaning that all elements along these dimensions are selected while s_x, s_y, and r_x are held constant.

Likewise, given $\mathbf{v} = (s_x, s_y, r_x)^{\mathrm{T}}$, we construct the set $\{\mathbf{v}, \mathcal{D}^{\text{obs}}(:, s_x, s_y, r_x, :)\}$ for our training process, whose objective function is defined as

$$J_2(\theta) = \sum_{s_x=1}^{S_x} \sum_{s_y=1}^{S_y} \sum_{r_x=1}^{R_x} \|(\mathcal{M}_\theta(\mathbf{v}) \circ \mathcal{P}(:, s_x, s_y, r_x, :) - \mathcal{D}^{\text{obs}}(:, s_x, s_y, r_x, :)\|_{\mathrm{F}}^2, \tag{7}$$

where S_x and S_y are the numbers of sources in the inline and crossline direction, respectively. In addition, R_x denotes the number of receivers in the inline direction. Additional details and results can be found in the synthetic data example.

We adopt a different profile selection approach when addressing the scenario involving common-midpoint (CMP) data with NMO. In this context, the application of NMO correction notably enhances event continuity across specific gathers, helping our network to capture their correlations effectively. An intuitive strategy is fixing m_x and m_y in the 5D seismic data set $\mathcal{Z}$ and extracting a 3D tensor $\mathcal{X}(t, h, \alpha)$. This tensor comprises traces gathered at the same CMP, where the different seismic traces exhibit similar structural characteristics. Consequently, such a slicing method enhances the homogeneity of the data within $\mathcal{X}$, which helps convolutional networks. For a more detailed comparison of the different profiles within $\mathcal{X}$, two distinct unfolding approaches are used, with the time dimension held constant. As shown in Figure 3, the tensor $\mathcal{X} \in \mathbb{R}^{I_1 \times I_2 \times I_3}$ can be unfolded into either matrix $\mathbf{X}_{(1)} \in \mathbb{R}^{I_1 \times I_2 I_3}$ or $\mathbf{X}_{(2)} \in \mathbb{R}^{I_1 \times I_3 I_2}$. It is widely recognized that the amplitude variations resulting from azimuthal anisotropy are generally less pronounced than those caused by changes in offset. The application of these unfolding methods to actual field data, as shown in Figure 4, also reveals that due to the variation in offset impacting event amplitude and arrival time, the unfolding method in Figure 4a results in more structurally coherent profiles compared with Figure 4b. Hence, we favor the unfolding strategy shown in Figure 3a (marked as U) to $\mathcal{X}$ and create a data set $\{\mathbf{v}, \mathbf{X}_{(1)}^{(m_x, m_y)}\}$ for self-supervised training, where $\mathbf{v} = (m_x, m_y)^{\mathrm{T}}$ is the input of our network and $\mathbf{X}_{(1)}^{(m_x, m_y)}$ is the corresponding learning target. The training process calculates the loss function only at positions with available observed data to optimize the network according to the following objective function:

$$J_3(\theta)=\sum_{m_x=1}^{M_x}\sum_{m_y=1}^{M_y}\|\mathcal{M}_\theta(\mathbf{v})\circ \mathrm{U}(\mathcal{P}_{:,m_x,m_y,:,:})-\mathbf{X}_{(1)}^{(m_x,m_y)}\|_{\mathrm{F}}^2, \quad (8)$$

where M_x and M_y are the largest lengths of the inline and crossline axes, respectively. After completing the training process, we process each $\mathbf{v}=(m_x,m_y)^{\mathrm{T}}$ to acquire its respective profile for seismic data reconstruction.

Network architecture with feature frequency modulation

We develop an innovative network structure to accommodate the profile-level output. This advancement primarily involves modifying the MLP framework by incorporating additional convolutional layers. As shown in Figure 5, the network architecture can be conceptually segmented into two main components. The first is a predefined single FFM layer $\gamma(\mathbf{v})$, implemented to improve positional encoding capabilities. The second component begins with an MLP-type encoder, which efficiently converts coordinates $\mathbf{v}$ into the corresponding latent variables ϕ. This process effectively encapsulates the fundamental attributes of the seismic profile. Subsequently, a convolutional network-based decoder reconstructs the full seismic profile from ϕ. Using N_τ to represent the combination of encoder and decoder, the network parameters τ are meticulously optimized to align with the observed data, and the comprehensive representation of the NeRSI network is $M_\theta(\mathbf{v})=N_\tau(\gamma(\mathbf{v}))$.

Input positional encoding mapping

Although neural networks are widely renowned for their ability to approximate universal functions (Hornik et al., 1989), substantial evidence suggests that standard MLP often faces challenges in capturing high-frequency variations. Specifically, inputting the raw data position $\mathbf{v}$ directly into an MLP tends to produce overly smoothed results, leading to the loss of high-frequency details in the reconstructed data (Tancik et al., 2020). Expanding $\mathbf{v}$ into its Fourier spectrum before feeding it into the MLP becomes a common practice to mitigate this issue. This method significantly improves the model's ability to detect and represent high-frequency signals, enhancing overall data fidelity. Accordingly, we propose integrating a positional encoding γ as a high-dimensional mapping defined by

$$\gamma_K(\mathbf{v})=[\cos(\omega_1 v_1),\sin(\omega_1 v_1),\cos(\omega_1 v_2),\sin(\omega_1 v_2),\ \ldots,\ \cos(\omega_K v_n),\sin(\omega_K v_n)]^{\mathrm{T}}, \quad (9)$$

where K represents the total number of components, and the ith frequency mapping can be either formulated by $\omega_i=i\pi/\beta$ with linear sampling or $\omega_i=\pi\beta^i$ with exponential sampling. Here, $\mathbf{v}$ represents an arbitrary coordinate vector normalized within $[0,1]$. Our experiments empirically find that using exponentially varying ω results in superior convergence for seismic signals.

To visually demonstrate the functionality of the FFM module, we carry out an experiment using a set of 100 sample points. These points were then subjected to coordinate normalization within the range of $[0,1]$. Moreover, we empirically set the parameters

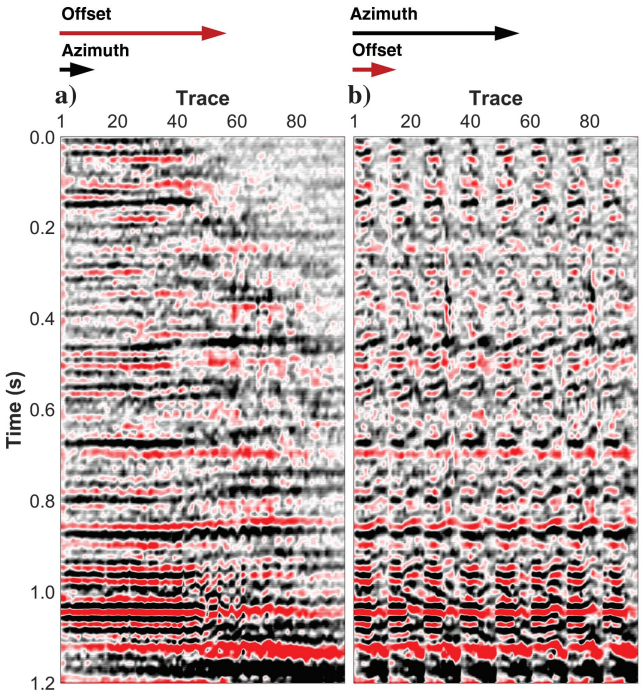

Figure 4. Field data examples of two different unfolding strategies. (a) The profile generated from common-offset azimuthal gathers and (b) the profile generated from azimuthal-sectored gathers.

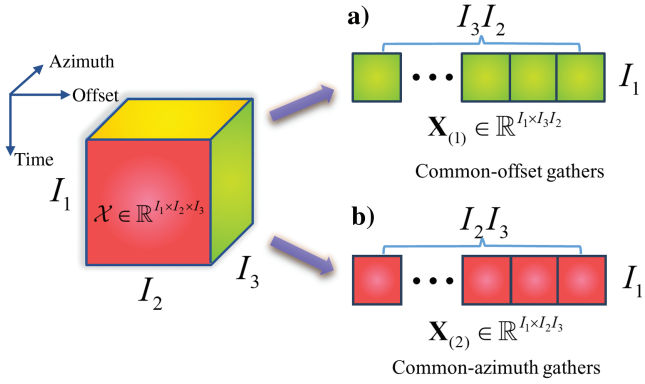

Figure 3. Two different unfolding strategies. (a) The profile generated from common-offset azimuthal gathers and (b) the profile generated from common-azimuth gathers.

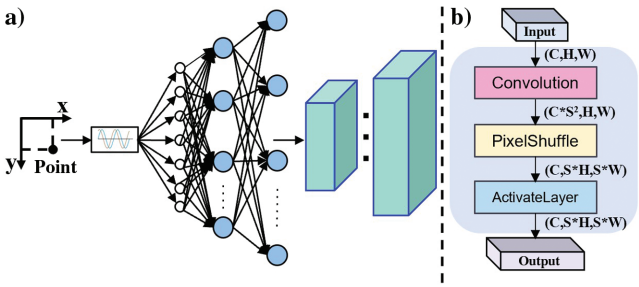

Figure 5. The proposed profile-wise NeRSI interpolation method. (a) Profile-wise implicit representation takes the position index as input and uses an MLP + convolutional neural network to output the entire image in the specified dimensions from the compressed latent space ϕ. (b) The architecture of the NeRSI block designed to upscale the feature map by a factor of S.

$K = 40$ and $\omega_i = \pi \times 1.25^i$ in equation 9. Following these preprocessing steps, we use positional encoding on the normalized coordinates to generate the results shown in Figure 6. Each column in Figure 6 shows the positional encoding of a sample point. Notably, this encoding procedure serves to convert the original low-dimensional coordinates into a high-dimensional Fourier feature space. Such a transformation is advantageous as it enhances the network's capacity to capture the high-frequency components inherent in the data effectively, a phenomenon well documented in seminal studies such as NeRF (Martin-Brualla et al., 2021).

To provide a clearer demonstration of the efficacy of FFM, we conduct a comparative analysis with two MLP networks, one augmented with the FFM module and the other without it, to model identical 2D seismic data. These networks are identical except for the inclusion of positional coding. After training for 80 epochs, we present the results for both scenarios in Figure 7. The outcomes distinctly showcase the network's struggle to fit the data in the absence of FFM accurately. In contrast, the incorporation of FFM enables us to achieve a fitting outcome that closely resembles the original data. Although we acknowledge that with increased iterations, the FFM-less network may also start to exhibit effective structures, the initial findings underscore the advantage of FFM in facilitating rapid network feature extraction. This experiment serves as a direct demonstration of the pivotal role played by the FFM module in our proposed methodology.

Hence, we incorporate the FFM module into our methodology. By adapting the frequency mapping to an exponential variation, our method effectively captures the high-frequency variations inherent in seismic signals, thereby enhancing overall interpolation performance and accuracy.

NeRSI network architecture

Using a point-wise MLP decoder to generate all point values of seismic data is inefficient, particularly for large data sets, Chen et al. (2021a) introduce a neural network implicit representation for video compression. This novel approach inputs a normalized timestamp "t" to produce the corresponding image at that instant. Through training, the network encapsulates the entirety of the video, demonstrating a significant advancement in data compression and retrieval efficiency.

Inspired by the NeRV model, we adapt their network structure to develop a specialized architecture for interpolating 5D seismic data, termed NeRSI. The NeRSI architecture, as shown in Figure 5a, comprises the MLP encoder followed by multiple NeRSI blocks that contain convolutional layers. By integrating these blocks behind the MLP, we can leverage shared convolutional kernels to produce all points in the output profile simultaneously, enhancing the efficiency and effectiveness of the framework. In addition, to efficiently capture the mapping function $N_\tau(\cdot)$ between encoded coordinates and seismic profiles, we adopt a similar approach from StyleGAN (Karras et al., 2019) for its advanced pattern and detail recognition capabilities. Specifically, we introduce nonlinear transformation layers to condense the encoded coordinates $\Gamma(\mathbf{v})$ to the latent variable ϕ. This latent variable ϕ functions as a compact representation in the mapping process, enhancing the model's efficiency and accuracy in interpreting complex seismic data.

The NeRSI blocks, shown in Figure 5b, serve as the decoder for the output seismic profile from ϕ. To preserve the output dimension, it adopts the PixelShuffle technique (Shi et al., 2016) for the upscaling process. Moreover, convolution and activation layers are integrated to enhance network expressiveness. Undoubtedly, NeRSI is a compact and lightweight network model that uses coordinate embedding to generate the corresponding profiles. The profile-wise approach significantly improves efficiency. In addition, the self-supervised learning procedure eliminates the requirement for extra-labeled data, rendering the NeRSI method exceptionally suitable for field seismic data interpolation tasks.

Nuclear norm regularization

The performance of equation 8 is satisfactory for noise-free data. However, field data are always contaminated by noise, complicating the accurate discernment of useful signals. Another notable challenge is the network's tendency to fit this noise, leading to outputs riddled with noisy reconstructions. As we discussed previously, seismic signals typically exhibit low-rank characteristics. Incorporating this intrinsic property into our objective function will more effectively extract the desired events and significantly improve denoising performance.

As a convex relaxation form of low-rank regularization, nuclear norm regularization is a widely used technique designed to enhance the generalization capability of models while controlling their complexity. Therefore, we also integrate nuclear norm regularization into our method. The nuclear norm of the matrix $\mathbf{X}$ is defined as follows:

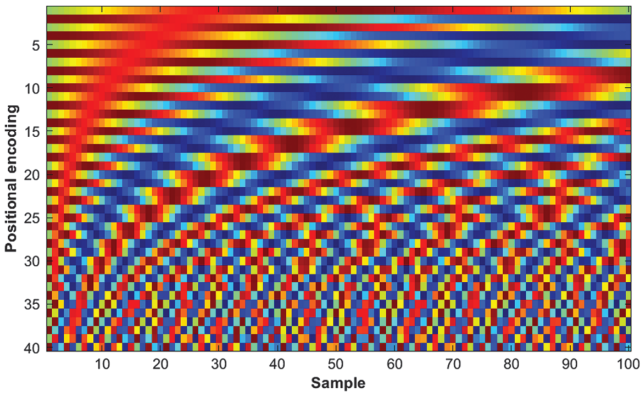

Figure 6. Position encoding results of 100 samples.

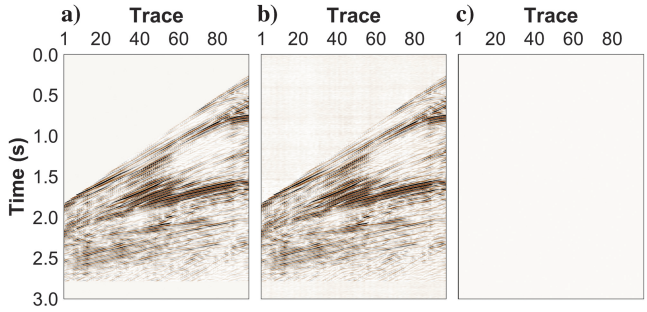

Figure 7. Positional coding validation. (a) Original 2D seismic signal, covering 3.84 km with a 40 m trace interval, (b) results obtained using an MLP with positional coding, and (c) results obtained using an MLP without positional coding. The MLP exhibits significant difficulty in extracting reflections with the same number of training epochs.

$$\|\mathbf{X}\|_* = \sum_{i=1}^{k} \sigma_i, \tag{10}$$

where $\sigma_1, \sigma_2, \ldots,$ and σ_k are the ordered singular values of $\mathbf{X}$. By incorporating this regularization into our original loss function in equation 8, a modified objective function for noisy data reconstruction is formulated as follows:

$$J_4(\theta) = \sum_{m_x=1}^{M_x} \sum_{m_y=1}^{M_y} \|\mathcal{M}_\theta(\mathbf{v}) \circ \mathrm{U}(\mathcal{P}_{:,m_x,m_y,:,:}) - \mathbf{X}_{(1)}^{(m_x,m_y)}\|_F^2 + \lambda \|\mathcal{M}_\theta(\mathbf{v})\|_*, \tag{11}$$

where the notation $\|\cdot\|_*$ denotes the nuclear norm, and λ is a hyperparameter for balancing the loss components. By selecting an appropriate weight λ, we can ensure that the network's output satisfies the low-rank assumption during training, thereby enhancing the model's robustness to noise. After training, we process each $\mathbf{v} = (m_x, m_y)^{\mathrm{T}}$ to acquire its respective profile for seismic data reconstruction. Our method not only fits the seismic profiles but also harnesses data redundancy and wavefield consistency to reduce the impact of noise effectively. A balance is achieved between fidelity to observations and regularization, leading to optimal output results.

EXPERIMENTS

Synthetic data example

We first use an open 5D seismic data set (Society of Exploration Geophysicists, 2024) with manual decimation to validate the effectiveness of the coordinate-based neural implicit representation approach in seismic data interpolation. This 5D seismic data set comprises 51 sail lines, each with 96 shots and eight cables per shot with 68 receivers per streamer. There are 625 samples along the time dimension with an 8 ms time interval. Consequently, it has a data size of $625 \times 51 \times 96 \times 8 \times 68$. In addition, the data are not corrected by NMO, thereby posing a significant challenge for data reconstruction algorithms. Our focus is on sail lines 25 to 41, from which we generate the data set $\mathcal{O}(t, s_x, s_y, r_x, r_y)$ of size $384 \times 16 \times 32 \times 8 \times 32$ to validate the proposed methods. To simulate real-world seismic data scenarios involving missing traces, we use a masking process that randomly removes seismic traces. In our experimental setup, we deliberately eliminate 80% of seismic traces, resulting in a highly sparse data set, denoted as $\mathcal{O}^{\mathrm{obs}}$. This deliberate sparsity simulates the challenges often encountered in seismic data processing, providing a rigorous test for our proposed methods.

Then, we use the point-wise method (Liu et al., 2024) shown in Figure 2 to reconstruct the decimated seismic data. Specifically, we use a 17-layer MLP network with 384 neurons in the hidden layer. Within the FFM module, we opt for $L = 10$ for encoding each input coordinate, with the frequency ω varying exponentially. During the self-supervised training process, the network mentioned previously exhibits ample network capacity. This allows us to directly encode the entire $\mathcal{O}^{\mathrm{obs}}$ into the MLP, bypassing the need for sliding overlapping window processing typically used in traditional methods. After training, we query each coordinate point to obtain its corresponding seismic amplitude value.

Despite its efficacy in recovering missing traces, the point-wise training strategy, which operates on a point-by-point basis, is not sufficient. To address this, we apply the proposed profile-wise method, NeRSI, to reconstruct the preceding data. Specifically, the strategy described in equation 7 is used to extract slices of $\mathcal{O}^{\mathrm{obs}}$ to construct a training set consisting of 4096 ($16 \times 32 \times 8$) seismic profiles. In the FFM module shown in Figure 5, we use an exponential variation of the frequency ω and set $K = 40$ for encoding each input coordinate. The encoder includes two fully connected layers, and the decoder comprises three NeRSI modules, each with an upsampling rate of two. It is worth noting that we do not use the nuclear norm in this example because the data set is clean.

The S/Ns of the results obtained from the preceding two methods are presented in Table 1. This table reveals that, overall, the profile-wise method achieves an S/N that is 2.88 dB higher than the point-wise method while also processing the data 40 times faster. We select an effective conventional baseline method, PMF-TR (Liu et al., 2022), for further comparison. The comparative results are shown in Figure 8. Figure 8a shows eight gathers from the complete data with $s_x = 16$, $r_y = 32$, s_y ranging from 1 to 16, and r_x ranging from 1 to 8. We can see that the original data comprise horizontal and dipping events, presenting a challenge for reconstruction. Figure 8b plots the decimated data with 80% irregularly missing traces. The recovered results by PMF-TR, the point-wise method (Liu et al., 2024), and the proposed profile-wise method are shown in Figure 8c, 8e, and 8g, respectively, with the corresponding reconstruction errors shown in Figure 8d, 8f, and 8h. All three methods are effective in data interpolation. Quantitative calculations reveal S/Ns of 12.37, 16.61, and 18.67 dB for the PMF-TR method, the point-wise method, and the profile-wise method, respectively. Both implicit representation methods outperform the PMF-TR method, demonstrating the superior performance of these networks. Furthermore, as indicated by the blue arrows, the dipping structure in the complete data is not fully recovered by the PMF-TR and point-wise methods. In the area marked by the yellow arrows, it is apparent that the PMF-TR method and the point-wise method exhibit useful signal leakage. In contrast, the profile-wise method proposed in this paper successfully recovers the dipping structure and does not have an obvious leakage of useful signals. This may be attributed to the convolutional network-style decoder of the profile-wise method, which has a larger receptive field, thus providing superior feature extraction ability for reconstructing data with complex structures.

To summarize, through testing on synthetic data with complex structures and a high rate of missing values, the proposed method leverages unsupervised learning to thoroughly examine the continuous wavefield of synthetic data, yielding excellent reconstruction results while maintaining high efficiency. Notably, it effectively reconstructs seismic data without NMO, showcasing the network's impressive ability to capture the inherent structure of seismic data. Visually and quantitatively, the proposed method outperforms traditional methods.

Table 1. Evaluation of point-wise and profile-wise reconstruction methods on synthetic data.

Method	S/N (dB)	Training time (min)	Testing time (s)	Total time consumption (min)
Point-wise	12.88	890	600	900
Profile-wise	15.16	21	75	22.25

To further demonstrate our proposed unsupervised interpolation method, we use synthetic data to compare with two existing algorithms, SSLI (Fang et al., 2023a) and DPSI (Kong et al., 2020). Specifically, we use 5D data $\mathcal{O}(t, s_x, s_y, r_x, r_y)$ as described previously, with dimensions $384 \times 16 \times 32 \times 8 \times 32$, wherein 70% of seismic traces are randomly removed to simulate real-world data gaps. Because DPSI is limited to 3D data, we extract a 3D subset with dimensions $384 \times 32 \times 32$ from $\mathcal{O}(t, s_x, s_y, r_x, r_y)$ by setting $s_x = 8$ and $r_x = 4$ for testing purposes. For the SSLI method, we extract 20,000 $32 \times 32 \times 32$ 3D cubes from $\mathcal{O}(t, s_x, s_y, r_x, r_y)$ to train the network. After training, we use the network to process the entire $\mathcal{O}(t, s_x, s_y, r_x, r_y)$ and extract the same portion corresponding to the DPSI method for comparison. Specifically, we compare the extracted portion from our results against those from SSLI and DPSI, displaying the outcomes in two dimensions, as shown in Figure 9. All three methods effectively reconstruct the missing seismic traces. However, our method demonstrates the least signal leakage when comparing the residual results.

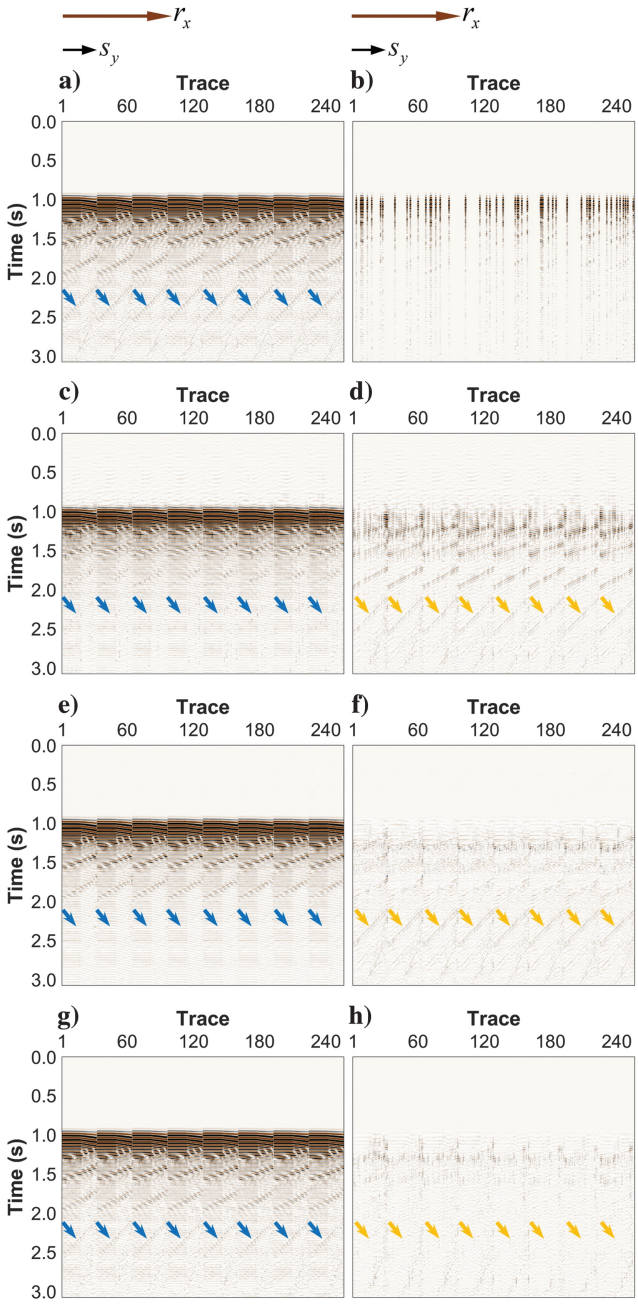

Figure 8. A comparison of the results obtained using different methods to reconstruct synthetic data. (a) Eight gathers from the complete data, each with an 80 m trace interval; (b) decimated data with 80% of traces irregularly missing; (c and d) the recovered results and reconstruction errors using the PMF-TR method, respectively; (e and f) the recovered results and reconstruction errors using the point-wise method, respectively; and (g and h) the recovered results and reconstruction errors using the profile-wise method, respectively. The blue arrows indicate the incomplete recovery of the dipping structure in the complete data by the PMF-TR and point-wise methods. Both methods exhibit signal leakage in the region marked by the yellow arrows. In contrast, our profile-wise method performs better, effectively recovering the dipping structure in the complete data without significant signal leakage.

Table 2 shows a quantitative comparison, showing DPSI achieving an S/N of 12.04 dB, SSLI at 15.53 dB, and our method achieving 17.16 dB. Moreover, our approach boasts higher efficiency. For the 5D data $\mathcal{O}(t, s_x, s_y, r_x, r_y)$ of size $384 \times 16 \times 32 \times 8 \times 32$, NeRSI and SSLI require 22 and 44 minutes, respectively, to finish the training and testing. On average, for a 3D cube of size $384 \times 32 \times 32$, NeRSI, SSLI, and DPSI require 10 s, 20 s, and 11 min on the same graphics processing unit, respectively. Compared with DPSI and SSLI, our method directly processes 5D data and outputs by profile with high efficiency. It surpasses other unsupervised learning methods in the reconstructed data's S/N ratio and processing speed, fully showcasing the potential of our method in seismic data interpolation.

Field data experiment

Compared with synthetic data, field data exhibit greater complexity and are significantly affected by noise, posing considerable challenges for network training. We also choose PMF-TR as a baseline method to evaluate the effectiveness of our proposed profile-wise reconstruction methods and use the same land data set obtained in Canada for comparison (Liu et al., 2022). Similarly, we first organize the irregularly sampled acquisition data into grids. Each grid has a CMP area of 20 m × 20 m, an offset of 400 m, and an azimuth of 45°. Within each grid, we compute the average of the traces falling within it. After this binning process, the binned data consist of 601 time samples, 38 CMP x-points, 76 CMP y-points, 12 offsets, and eight azimuths. As a result, we refer to the incomplete 5D field seismic data set as $\mathcal{D}^{\text{obs}}(t, m_x, m_y, |\mathbf{h}|, Az)$, where $|\mathbf{h}| = \sqrt{h_x^2 + h_y^2}$ and $Az = \arctan(h_x/h_y)$. Notably, this field example exhibits a trace-missing ratio of 94.39%.

For this data set, we use an exponential variation of the frequency ω and choose $K = 80$ to encode each input coordinate in the FFM module. The encoder has two fully connected layers. For decoding the intermediate latent variables ϕ, we use three NeRSI modules

Table 2. Evaluation of three unsupervised reconstruction methods on synthetic data.

Method	S/N (dB)	Average time consumption
DPSI	12.04	11 min
SSLI	15.53	20 s
NeRSI	17.16	10 s

with upsampling rates of five, two, and two, respectively. Subsequently, we construct a training set consisting of 2888 (38 × 76) seismic profiles, as per the method outlined in Figure 3a. The model is then trained following equation 11.

Figure 10 shows a slice view of the reconstruction results using the PMF-TR and NeRSI methods for these field data. Specifically, Figure 10a shows CMP *y*-sections of the observed 5D volume with a fixed offset (bin 6 = 2.4 km) and azimuth (bin 4 = 135°). The original data section contains a significant number of missing traces and noise, presenting a considerable challenge for reconstruction. Figure 10b shows the CMP *y*-section results obtained by PMF-TR, wherein the missing content in Figure 10a is effectively recovered. However, some noise interference persists in the shallow layer, obscuring the desired events. Figure 10c shows the results from NeRSI, wherein all missing traces in Figure 10a are accurately recovered. Compared with the PMF-TR method, in the middeep region, approximately 0.6 to 1 s, the two methods have similar results. However, in the shallow position, due to the extremely low S/N of the original data, the events obtained by PMF-TR are drowned out by random noise, and the NeRSI method achieves a higher S/N and provides more pronounced events. To further validate the effectiveness of the proposed method, we fix CMP *x* (bin 4 = 0.08 km) and offset (bin 6 = 2.4 km) and examine the results from a different perspective. Figure 11a shows the sections of the original seismic records, which exhibit larger gaps compared with Figure 10a. Figure 11b and 11c shows the result obtained from the PMF-TR method and the proposed method, respectively. The NeRSI method effectively recovers the missing traces, even in locations with significant gaps, suggesting that the network has truly learned the intrinsic 5D wavefield. Compared with the PMF-TR method, both methods yield impressive results in the region highlighted by the blue box in Figure 11, whereas the NeRSI method demonstrates superior lateral consistency in recovered reflections. However, within the area marked by the red box, significant noise is observed in the results from the PMF-TR method. In contrast, using the NeRSI method leads to a more pronounced enhancement of horizontal continuity in the reconstruction results and exhibits better robustness to noise while performing data interpolation. In addition, our analysis revealed that the NeRSI method brings to light more faint events that were previously overshadowed by noise in the PMF-TR results. This means that our method not only maintains critical data but also unveils additional geologic information that can be obscured by noise in other methods. Thus, we believe that the NeRSI method offers a more robust and comprehensive approach to seismic data analysis.

For a comprehensive comparison, Figure 12a shows the stacking data before interpolation. The original stacking data have a notably low S/N, and many reflections are obscured by noise, particularly in the shallow-layer regions. The reconstructed stacking cubes obtained using the PMF-TR and NeRSI methods, as shown in Figure 12b and 12c, respectively, effectively eliminate prestack noise and

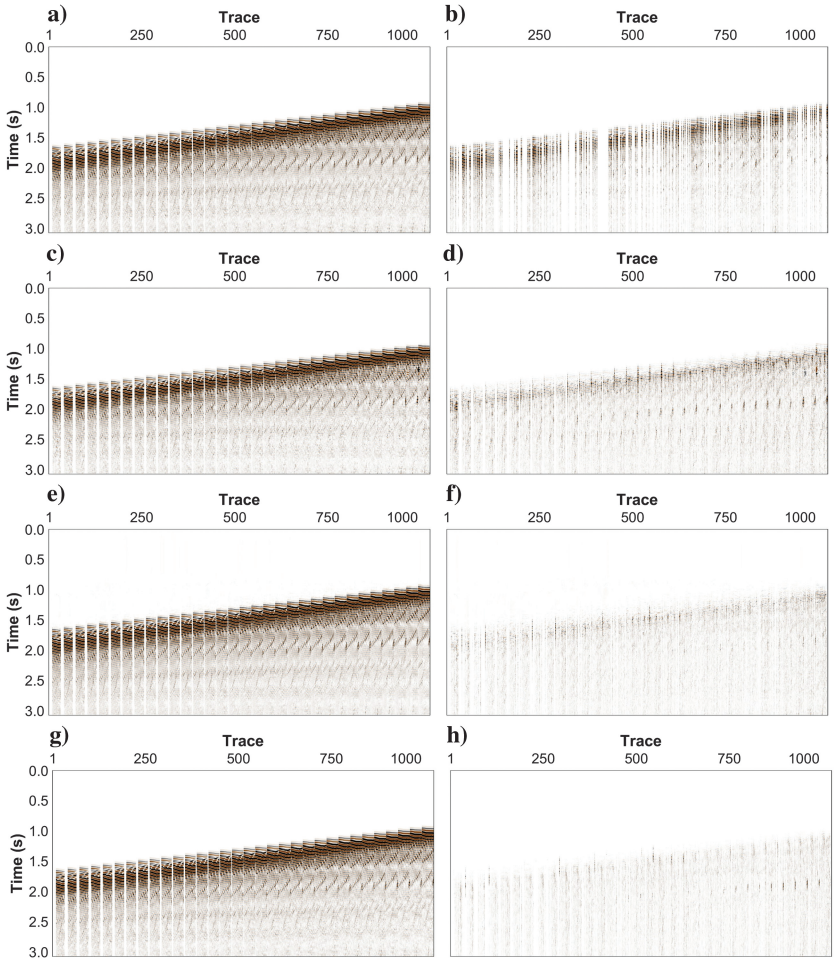

Figure 9. A comparison of the results obtained using different unsupervised methods to reconstruct synthetic data. (a) Complete data with an 80 m trace interval; (b) decimated data with 70% of traces irregularly missing; (c and d) the recovered results and reconstruction errors using the DPSI method, respectively; (e and f) the recovered results and reconstruction errors using the SSLI method, respectively; and (g and h) the recovered results and reconstruction errors using the profile-wise method, respectively.

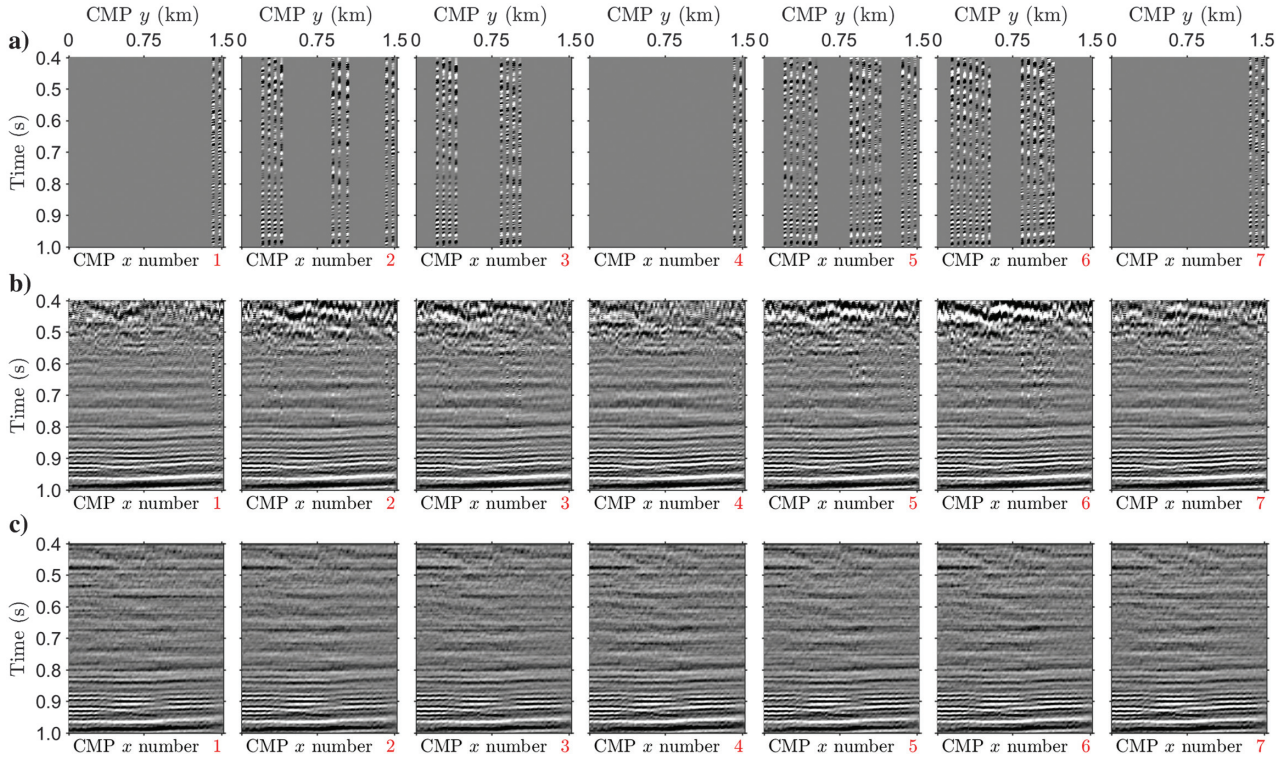

Figure 10. A slice view of the CMP y gather results of the seismic data by assigning offset = 2.4 km and azimuth = 135°. (a) The original field data with CMP x-intervals of 20 m, (b) the results of reconstruction using the PMF-TR method, and (c) the results of reconstruction using the NeRSI method.

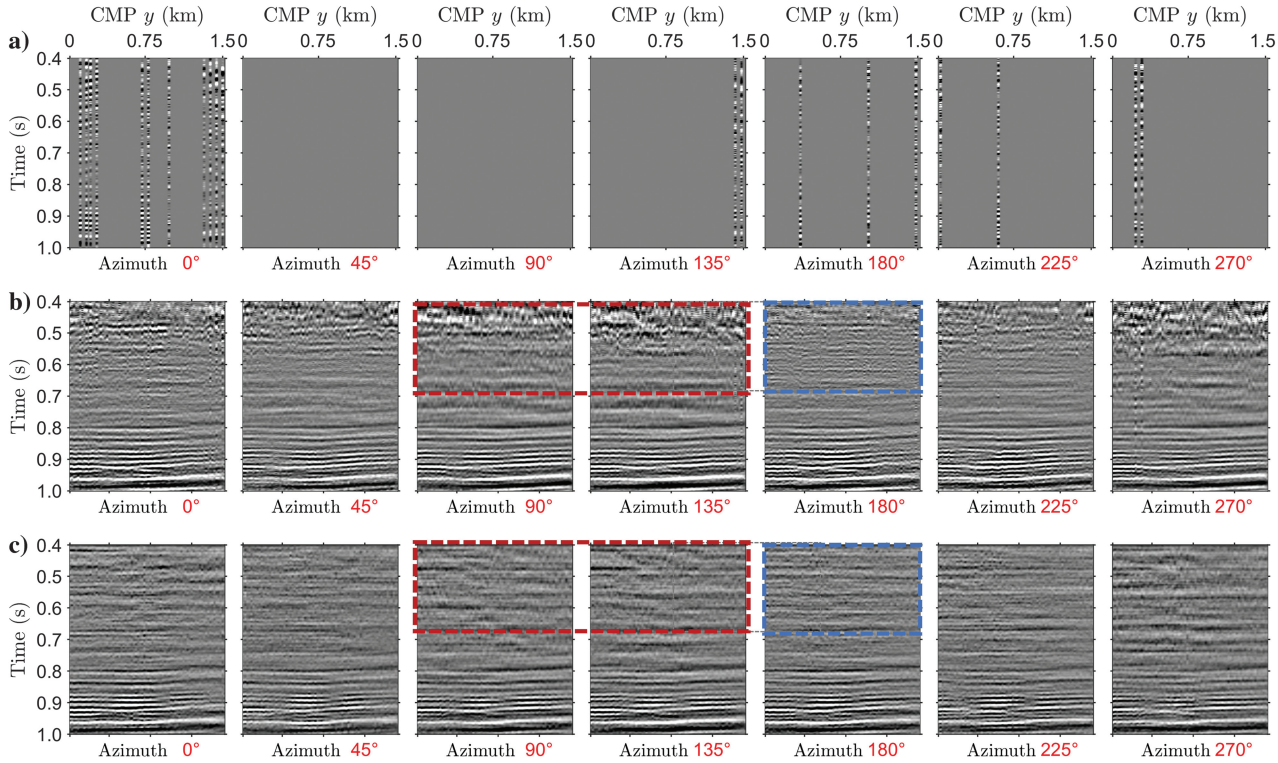

Figure 11. A slice view of CMP y-gather results by assigning offset = 2.4 km and CMP $x = 0.08$ km. Azimuth bin $[1, 8]$ is equivalent to [0°, 315°] with an increase of 45°. (a) The original field data, (b) the results of reconstruction using the PMF-TR method, and (c) the results of reconstruction using the NeRSI method.

significantly enhance the signal energy compared with the original stacking data in Figure 12a. However, the profiles shown in Figure 12b still display slight residual noise in the shallow-layer region. In contrast, a very low level of random noise can be observed in the profiles shown in Figure 12c, thereby confirming the effectiveness of the proposed NeRSI method in recovering noisy and irregularly sampled seismic data.

In addition, to demonstrate the effectiveness of our method in suppressing noise while preserving essential structural information within the data, we conducted an exhaustive stacking analysis on a region rich in patterns using the same network. The positional encoding length is chosen with $K = 120$, and the regularization factor λ is $5e^{-5}$. The stacking results before and after reconstruction are shown in Figure 13. Figure 13a is the stacking result before reconstruction, and Figure 13b is the stacking result after reconstruction using the NeRSI method. These results show that our approach preserves the prominent structural features of the original stacking results. The regions within the red, green, and blue boxes are selected for detailed magnification. In the area marked by the red box, the events previously obscured by noise before reconstruction became clear. Within the green box, the faint events were enhanced while maintaining their structure before reconstruction. In the region demarcated by the blue box, the enhancement of horizontal event energy is observed, with the steeply dipping events, indicated by the yellow arrow, being well preserved. Compared with the prereconstruction state, the structure became significantly clearer. This observation underscores that the NeRSI method effectively suppresses noise without compromising the preservation of crucial data structures, further demonstrating the potential of the NeRSI method in actual 5D seismic data interpolation.

Ablation experiment

In Figures 10 and 11, it is evident that the data recovered by the NeRSI method exhibit a higher S/N. One contributing factor is that the network is trained to fit 2888 profiles simultaneously during training. The consistent nature of seismic wavefields enables the effective utilization of redundancy in the 5D data to mitigate the impact of noise. A more pivotal factor is the selection of structurally well-defined profiles as the network output and the application of nuclear norm regularization. In equation 11, the fidelity term forces the model output to approximate the observations closely. However, the observations often contain significant noise. In contrast, the nuclear norm regularization imposes a constraint on the model to output a profile with as small a rank as possible, thereby achieving a higher S/N. By carefully selecting an appropriate value for λ by grid search, a balance can be struck between the fidelity term and the regularization term, leading to satisfactory reconstruction results.

To validate the effect of the nuclear norm regularization, we select other 5D field data collected in China (Chen et al., 2021c). This data set consists of 250 temporal samples with a sampling rate of 4 ms, 10 midpoint x-samples, 10 midpoint y-samples, 21 offset x-samples, and 10 offset y-samples. The proportion of the missing traces in the data set is as high as 82%. We set $\lambda = 0$ and $\lambda = 1e^{-4}$ in equation 11 to train the model and reconstruct the field data, respectively. In Figure 14, we present a set of original CMP gathers with CMP $x = 2$ and CMP $y = 2$. These gathers collectively form a profile with dimensions of 250×210, covering a range of 21 offset x-samples and 10 offset y-samples. Figure 14b corresponds to the reconstruction results without nuclear norm regularization

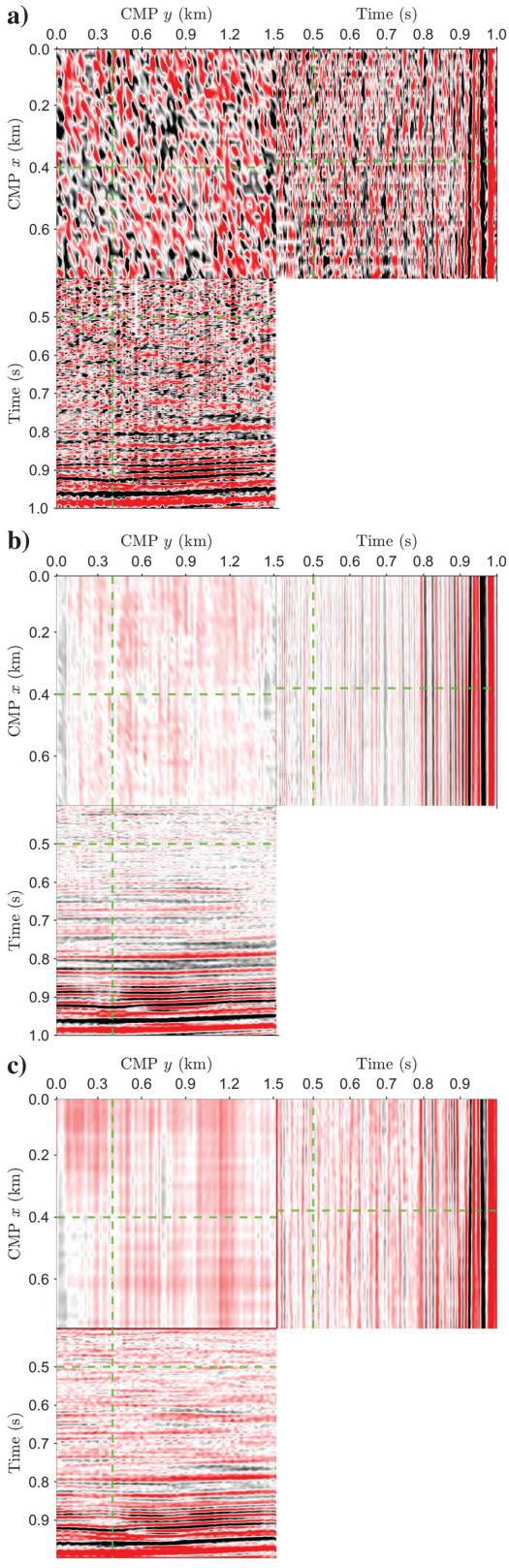

Figure 12. Stacking result comparisons. (a) Before reconstruction, (b) after reconstruction using the PMF-TR method, and (c) after reconstruction using the NeRSI method.

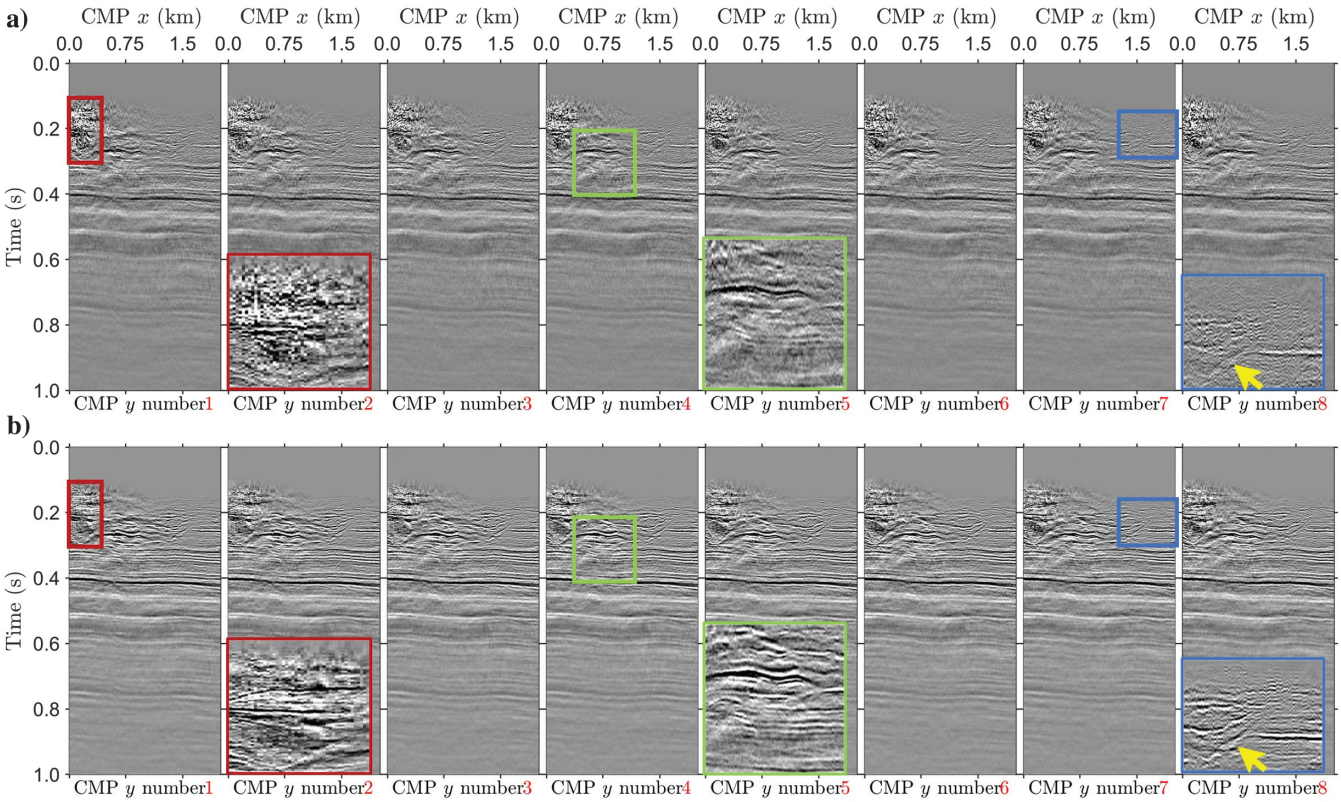

Figure 13. Large-scale stacking result comparison from the same work area of Figure 10. (a) Before reconstruction and (b) after reconstruction using the NeRSI method. The areas within the red, green, and blue boxes are selected representative patterns for detailed magnification. Compared with the yellow arrowed areas, the diffraction waves are well preserved.

Figure 14. A test of the effect of nuclear norm regularization. (a) The incomplete seismic data with an 80 m trace interval, (b) the reconstruction results without nuclear norm regularization, and (c) the reconstruction results with nuclear norm regularization.

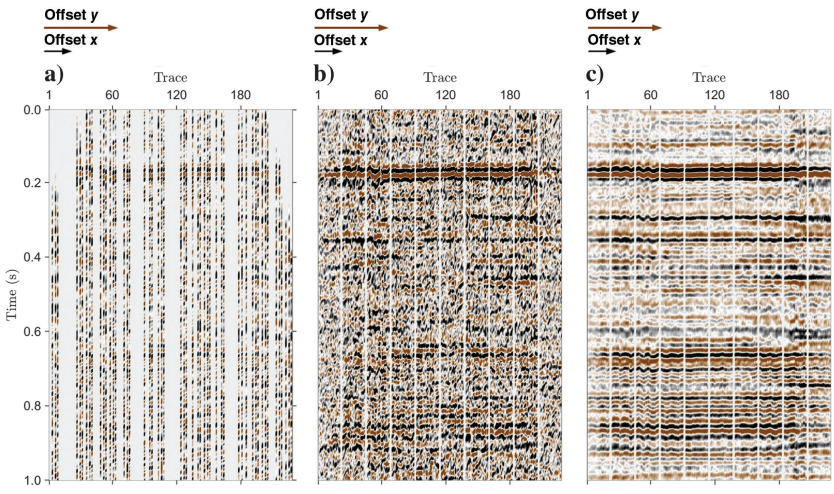

($\lambda = 0$), whereas Figure 14c corresponds to the reconstruction results with $\lambda = 1e^{-4}$. Comparing Figure 14b with Figure 14c, it is clear that as λ changes from 0 to $1e^{-4}$, the reconstruction results exhibit reduced noise interference and more coherent, continuous reflection events. This highlights the effectiveness of using nuclear norm constraints. However, when λ exceeds a certain threshold, we notice a slight degradation in the quality of reconstruction, indicating the need for a careful balance between data fidelity and regularization.

CONCLUSION

We leverage implicit neural representation to establish a self-supervised learning-based 5D seismic data interpolation model. By training an MLP network with limited samples from observed data, the entire seismic wave field is encoded into the MLP's weights. Querying this network on the wavefield at locations with missing data allows for reconstructing the complete data set. To enhance the efficiency of the model, we propose a novel network structure that

uses a convolutional network serving as the decoder to produce seismic profiles. This technique achieves a speed improvement of 40 times compared with the point-wise prediction method. In addition, a nuclear norm constraint is applied to the seismic profiles to boost the model's robustness against noise. The experiments in synthetic and field data indicate the effectiveness of the model in handling data with high missing rates and complex structures. These results also reveal the significant potential of coordinate-based models for efficient seismic data interpolation. Future work will focus on offgrid seismic data interpolation.

ACKNOWLEDGMENTS

This work was supported in part by the National Key Research and Development Program of China under grant 2021YFA0716903, in part by the National Natural Science Foundation of China under grant 42374135, and in part by the Fundamental Research Funds for the Central Universities under grant xzy012023073. The contribution of the second author is supported by the industrial sponsors of the Signal Analysis and Imaging Group (SAIG) consortium at the University of Alberta.

DATA AND MATERIALS AVAILABILITY

Data associated with this research are available and can be obtained by contacting the corresponding author.

REFERENCES

Bardan, V., 1987, Trace interpolation in seismic data processing: Geophysical Prospecting, **35**, 343–358, doi: 10.1111/j.1365-2478.1987.tb00822.x.

Chen, H., B. He, H. Wang, Y. Ren, S. N. Lim, and A. Shrivastava, 2021a, Nerv: Neural representations for videos: Advances in Neural Information Processing Systems, 21557–21568.

Chen, W., L. Yang, H. Wang, and Y. Chen, 2021b, Fast high-resolution hyperbolic radon transform: IEEE Transactions on Geoscience and Remote Sensing, **60**, 1–18, doi: 10.1109/TGRS.2020.3034752.

Chen, Y., S. Fomel, H. Wang, and S. Zu, 2021c, 5D dealiased seismic data interpolation using nonstationary prediction-error filter: Geophysics, **86**, no. 5, V419–V429, doi: 10.1190/geo2020-0540.1.

Chen, Y., S. Liu, and X. Wang, 2021d, Learning continuous image representation with local implicit image function: Proceedings of the IEEE/CVF Conference on Computer Vision and Pattern Recognition, 8628–8638.

Chen, Y., D. Zhang, Z. Jin, X. Chen, S. Zu, W. Huang, and S. Gan, 2016, Simultaneous denoising and reconstruction of 5-D seismic data via damped rank-reduction method: Geophysical Journal International, **206**, 1695–1717, doi: 10.1093/gji/ggw230.

Crawley, S., R. Clapp, and J. Claerbout, 1999, Interpolation with smoothly nonstationary prediction-error filters: 69th Annual International Meeting, SEG, Expanded Abstracts, 1154–1157, doi: 10.1190/1.1820707.

Da Silva, C., and F. J. Herrmann, 2015, Optimization on the hierarchical tucker manifold-applications to tensor completion: Linear Algebra and its Applications, **481**, 131–173, doi: 10.1016/j.laa.2015.04.015.

Downton, J., D. Holy, D. Trad, L. Hunt, S. Reynolds, and S. Hadley, 2010, The effect of interpolation on imaging and azimuthal AVO: A Nordegg case study: 80th Annual International Meeting, SEG, Expanded Abstracts, 383–387, doi: 10.1190/1.3513648.

Ely, G., S. Aeron, N. Hao, and M. E. Kilmer, 2015, 5D seismic data completion and denoising using a novel class of tensor decompositions: Geophysics, **80**, no. 4, V83–V95, doi: 10.1190/geo2014-0467.1.

Fang, W., L. Fu, M. Wu, J. Yue, and H. Li, 2023a, Irregularly sampled seismic data interpolation with self-supervised learning: Geophysics, **88**, no. 3, V175–V185, doi: 10.1190/geo2022-0586.1.

Fang, W., L. Fu, W. Xu, A. Bian, and H. Li, 2023b, CCNet-5D: 5D convolutional neural network for seismic data interpolation: Geophysics, **88**, no. 4, V333–V344, doi: 10.1190/geo2022-0420.1.

Fomel, S., and Y. Liu, 2010, Seislet transform and seislet frame: Geophysics, **75**, no. 3, V25–V38, doi: 10.1190/1.3380591.

Gan, S., S. Wang, Y. Chen, Y. Zhang, and Z. Jin, 2015, Dealiased seismic data interpolation using seislet transform with low-frequency constraint: IEEE Geoscience and Remote Sensing Letters, **12**, 2150–2154, doi: 10.1109/LGRS.2015.2453119.

Gao, J., M. Sacchi, and X. Chen, 2013, A fast reduced-rank interpolation method for prestack seismic volumes that depend on four spatial dimensions: Geophysics, **78**, no. 1, V21–V30, doi: 10.1190/geo2012-0038.1.

Gao, J., A. Stanton, and M. D. Sacchi, 2015, Parallel matrix factorization algorithm and its application to 5D seismic reconstruction and denoising: Geophysics, **80**, no. 6, V173–V187, doi: 10.1190/geo2014-0594.1.

Goyes-Peñafiel, P., E. Vargas, C. V. Correa, Y. Sun, U. S. Kamilov, B. Wohlberg, and H. Arguello, 2023, Coordinate-based seismic interpolation in irregular land survey: A deep internal learning approach: IEEE Transactions on Geoscience and Remote Sensing, **61**, 5912812, doi: 10.1109/TGRS.2023.3290468.

Gulunay, N., and R. E. Chambers, 1996, Unaliased f-k domain trace interpolation (UFKI): 66th Annual International Meeting, SEG, Expanded Abstracts, 1461–1464, doi: 10.1190/1.1826390.

Hennenfent, G., L. Fenelon, and F. J. Herrmann, 2010, Nonequispaced curvelet transform for seismic data reconstruction: A sparsity-promoting approach: Geophysics, **75**, no. 6, WB203–WB210, doi: 10.1190/1.3494032.

Hornik, K., M. Stinchcombe, and H. White, 1989, Multilayer feedforward networks are universal approximators: Neural networks, **2**, 359–366, doi: 10.1016/0893-6080(89)90020-8.

Kabir, M. N., and D. Verschuur, 1995, Restoration of missing offsets by parabolic Radon transform: Geophysical Prospecting, **43**, 347–368, doi: 10.1111/j.1365-2478.1995.tb00257.x.

Karras, T., S. Laine, and T. Aila, 2019, A style-based generator architecture for generative adversarial networks: Proceedings of the IEEE/CVF Conference on Computer Vision and Pattern Recognition, 4401–4410.

Kong, F., F. Picetti, V. Lipari, P. Bestagini, X. Tang, and S. Tubaro, 2020, Deep prior-based unsupervised reconstruction of irregularly sampled seismic data: IEEE Geoscience and Remote Sensing Letters, **19**, 1–5, doi: 10.1109/LGRS.2020.3044455.

Kreimer, N., and M. D. Sacchi, 2012, A tensor higher-order singular value decomposition for prestack seismic data noise reduction and interpolation: Geophysics, **77**, no. 3, V113–V122, doi: 10.1190/geo2011-0399.1.

Krull, A., T.-O. Buchholz, and F. Jug, 2019, Noise2void-learning denoising from single noisy images: Proceedings of the IEEE/CVF Conference on Computer Vision and Pattern Recognition, 2129–2137.

Li, J., D. Liu, D. Trad, and M. Sacchi, 2024, Robust unsupervised 5D seismic data reconstruction on both regular and irregular grid: Geophysics, **89**, no. 6, 1–86, doi: 10.1190/geo2024-0098.1.

Liu, D., W. Gao, W. Xu, J. Li, X. Wang, and W. Chen, 2024, 5-D seismic data interpolation by continuous representation: IEEE Transactions on Geoscience and Remote Sensing, **62**, 1–11, doi: 10.1109/TGRS.2024.3431439.

Liu, D., M. D. Sacchi, and W. Chen, 2022, Efficient tensor completion methods for 5-D seismic data reconstruction: Low-rank tensor train and tensor ring: IEEE Transactions on Geoscience and Remote Sensing, **60**, 1–17, doi: 10.1109/TGRS.2022.3179275.

Liu, D., X. Wang, W. Chen, Y. Zhou, W. Wang, Z. Shi, C. Wang, and C. Xie, 2019a, 3D seismic waveform of channels extraction by artificial intelligence: 89th Annual International Meeting, SEG, Expanded Abstracts, 2518–2522, doi: 10.1190/segam2019-3216216.1.

Liu, J., G. Liu, and Y. Chou, 2019b, Seismic data reconstruction via complex shearlet transform and block coordinate relaxation: Journal of Seismic Exploration, **28**, 307–332.

Mandelli, S., F. Borra, V. Lipari, P. Bestagini, A. Sarti, and S. Tubaro, 2018, Seismic data interpolation through convolutional autoencoder: 88th Annual International Meeting, SEG, Expanded Abstracts, 4101–4105, doi: 10.1190/segam2018-2995428.1.

Martin-Brualla, R., N. Radwan, M. S. M. Sajjadi, J. T. Barron, A. Dosovitskiy, and D. Duckworth, 2021, NeRF in the wild: Neural radiance fields for unconstrained photo collections, *in* Proceedings of the IEEE/CVF Conference on Computer Vision and Pattern Recognition, 7210–7219.

Mildenhall, B., P. P. Srinivasan, M. Tancik, J. T. Barron, R. Ramamoorthi, and R. Ng, 2021, NeRF: Representing scenes as neural radiance fields for view synthesis: Communications of the ACM, **65**, 99–106, doi: 10.1145/3503250.

Mohamed, S., and B. Lakshminarayanan, 2016, Learning in implicit generative models: arXiv preprint, doi: 10.48550/arXiv.1610.03483.

Naghizadeh, M., and M. D. Sacchi, 2009, F-x adaptive seismic-trace interpolation: Geophysics, **74**, no. 1, V9–V16, doi: 10.1190/1.3008547.

Oliveira, D. A., R. S. Ferreira, R. Silva, and E. V. Brazil, 2018, Interpolating seismic data with conditional generative adversarial networks: IEEE Geoscience and Remote Sensing Letters, **15**, 1952–1956, doi: 10.1109/LGRS.2018.2866199.

Oropeza, V., and M. Sacchi, 2011, Simultaneous seismic data denoising and reconstruction via multichannel singular spectrum analysis: Geophysics, **76**, no. 3, V25–V32, doi: 10.1190/1.3552706.

Park, J. J., P. Florence, J. Straub, R. Newcombe, and S. Lovegrove, 2019, DeepSDF: Learning continuous signed distance functions for shape representation, *in* Proceedings of the IEEE/CVF Conference on Computer Vision and Pattern Recognition, 165–174.

.Porsani, M. J., 1999, Seismic trace interpolation using half-step prediction filters: Geophysics, **64**, 1461–1467, doi: 10.1190/1.1444650.
Society of Exploration Geophysicists, 2024, SEG C3 NA, https://wiki.seg.org/wiki/SEG_C3_NA, accessed 11 November 2024.
Shahidi, R., G. Tang, J. Ma, and F. J. Herrmann, 2013, Application of randomized sampling schemes to curvelet-based sparsity-promoting seismic data recovery: Geophysical Prospecting, **61**, 973–997, doi: 10.1111/1365-2478.12050.
Shi, W., J. Caballero, F. Huszár, J. Totz, A. P. Aitken, R. Bishop, D. Rueckert, and Z. Wang, 2016, Real-time single image and video super-resolution using an efficient sub-pixel convolutional neural network: Proceedings of the IEEE Conference on Computer Vision and Pattern Recognition, 1874–1883.
Siahkoohi, A., R. Kumar, and F. Herrmann, 2018, Seismic data reconstruction with generative adversarial networks: 80th Annual International Conference and Exhibition, EAGE, Extended Abstracts, doi: 10.3997/2214-4609.201801393.
Spitz, S., 1991, Seismic trace interpolation in the FX domain: Geophysics, **56**, 785–794, doi: 10.1190/1.1443096.
Sun, Y., J. Liu, M. Xie, B. Wohlberg, and U. S. Kamilov, 2021, Coil: Coordinate-based internal learning for imaging inverse problems: arXiv preprint, doi: 10.48550/arXiv.2102.05181.
Tancik, M., P. Srinivasan, B. Mildenhall, S. Fridovich-Keil, N. Raghavan, U. Singhal, R. Ramamoorthi, J. Barron, and R. Ng, 2020, Fourier features let networks learn high frequency functions in low dimensional domains: Advances in Neural Information Processing Systems, 7537–7547.
Trickett, S., L. Burroughs, A. Milton, L. Walton, and R. Dack, 2010, Rank-reduction-based trace interpolation: 80th Annual International Meeting, SEG, Expanded Abstracts, 3829–3833, doi: 10.1190/1.3513645.
Wang, B., X. Chen, J. Li, and J. Cao, 2015, An improved weighted projection onto convex sets method for seismic data interpolation and denoising: IEEE Journal of Selected Topics in Applied Earth Observations and Remote Sensing, **9**, 228–235, doi: 10.1109/JSTARS.2015.2496374.
Wang, H., W. Chen, Q. Zhang, X. Liu, S. Zu, and Y. Chen, 2021, Fast dictionary learning for high-dimensional seismic reconstruction: IEEE Transactions on Geoscience and Remote Sensing, **59**, 7098–7108, doi: 10.1109/TGRS.2020.3030740.
Wang, Y., B. Wang, N. Tu, and J. Geng, 2020, Seismic trace interpolation for irregularly spatial sampled data using convolutional autoencoder: Geophysics, **85**, no. 2, V119–V130, doi: 10.1190/geo2018-0699.1.
Wu, X., L. Liang, Y. Shi, and S. Fomel, 2019a, FaultSeg3D: Using synthetic data sets to train an end-to-end convolutional neural network for 3D seismic fault segmentation: Geophysics, **84**, no. 3, IM35–IM45, doi: 10.1190/geo2018-0646.1.
Wu, X., Y. Shi, S. Fomel, L. Liang, Q. Zhang, and A. Z. Yusifov, 2019b, FaultNet3D: Predicting fault probabilities, strikes, and dips with a single convolutional neural network: IEEE Transactions on Geoscience and Remote Sensing, **57**, 9138–9155, doi: 10.1109/TGRS.2019.2925003.
Xu, W., V. Lipari, P. Bestagini, W. Chen, and S. Tubaro, 2022, Interpolation of missing shots via plug and play method with CSGs trained deep denoiser: 83rd Annual International Conference and Exhibition, EAGE, Extended Abstracts, doi: 10.3997/2214-4609.202210351.
Xu, Y., R. Hao, W. Yin, and Z. Su, 2015, Parallel matrix factorization for low-rank tensor completion: Inverse Problems & Imaging, **9**, 601, doi: 10.3934/ipi.2015.9.601.
Xu, Z.-Q. J., 2020, Frequency principle: Fourier analysis sheds light on deep neural networks: Communications in Computational Physics, **28**, 1746–1767, doi: 10.4208/cicp.OA-2020-0085.
Yu, S., J. Ma, and W. Wang, 2019, Deep learning for denoising: Geophysics, **84**, no. 6, V333–V350, doi: 10.1190/geo2018-0668.1.
Yu, S., J. Ma, X. Zhang, and M. D. Sacchi, 2015, Interpolation and denoising of highdimensional seismic data by learning a tight frame: Geophysics, **80**, no. 5, V119–V132, doi: 10.1190/geo2014-0396.1.
Zhang, H., X. Yang, and J. Ma, 2020a, Can learning from natural image denoising be used for seismic data interpolation? Geophysics, **85**, no. 4, WA115–WA136, doi: 10.1190/geo2019-0243.1.
Zhang, K., G. Riegler, N. Snavely, and V. N. Koltun, 2020b, Nerf++: Analyzing and improving neural radiance fields, arXiv preprint arXiv:2010.07492.
Zhou, Y., J. Gao, W. Chen, and P. Frossard, 2016, Seismic simultaneous source separation via patchwise sparse representation: IEEE Transactions on Geoscience and Remote Sensing, **54**, 5271–5284, doi: 10.1109/TGRS.2016.2559514.
Zhu, L., E. Liu, and J. H. McClellan, 2015, Seismic data denoising through multiscale and sparsity-promoting dictionary learning: Geophysics, **80**, no. 6, WD45–WD57, doi: 10.1190/geo2015-0047.1.

Biographies and photographs of the authors are not available.